# Structural basis of the strict phospholipid binding specificity of the pleckstrin homology domain of human evectin-2

Seiji Okazaki,[a] Ryuichi Kato,[a] Yasunori Uchida,[b] Tomohiko Taguchi,[b] Hiroyuki Arai[b] and Soichi Wakatsuki[a]*

[a]Structural Biology Research Center, Photon Factory, Institute of Materials Structure Science, High Energy Accelerator Research Organization (KEK), Tsukuba, Ibaraki 305-0801, Japan, and [b]Department of Health Chemistry, Graduate School of Pharmaceutical Sciences, University of Tokyo, Tokyo 113-0033, Japan

Correspondence e-mail: soichi.wakatsuki@kek.jp

Evectin-2 is a recycling endosomal protein involved in retrograde transport. Its primary sequence contains an N-terminal pleckstrin homology (PH) domain and a C-terminal hydrophobic region. The PH domain of evectin-2 can specifically bind phosphatidylserine, which is enriched in recycling endosomes, and plays an essential role in retrograde transport from recycling endosomes to the trans-Golgi network. The structure of human evectin-2 PH domain in complex with $O$-phospho-L-serine has recently been reported and demonstrates how the head group of phosphatidylserine is recognized. However, it was not possible to elucidate from the structure why evectin-2 cannot bind phosphatidic acid or phosphatidylethanolamine, which share a common moiety with phosphatidylserine. Here, the crystal structure at 1.75 Å resolution of an apo form of human evectin-2 PH domain, in which the ligand-binding site is free from crystal packing and is thus appropriate for comparison with the structure of the complex, is reported. Comparison between the structures of the apo form and the $O$-phospho-L-serine complex revealed ligand-induced conformational change evoked by interaction between the carboxyl moiety of the head group of phosphatidylserine and the main-chain N atom of Thr14. This structural change effectively explains the strict ligand specificity of the PH domain of human evectin-2.

## 1. Introduction

Retrograde transport from the plasma membrane to the trans-Golgi network (TGN) is crucial for a diverse range of cellular functions (Bonifacino & Rojas, 2006; Johannes & Popoff, 2008). A notable example is retrograde transport from early endosomes to recycling endosomes (REs) and subsequently to the TGN. The physiological function of this pathway is to recycle several Golgi proteins from REs to the TGN in order to maintain their Golgi localization. This pathway is exploited by protein toxins that are secreted by bacteria (for example, Shiga toxin and cholera toxin; Sandvig & van Deurs, 2002).

Evectin-2 has been identified as a post-Golgi-localized protein that is widely expressed in several tissues (Krappa et al., 1999). Evectin-2 consists of an N-terminal pleckstrin homology (PH) domain and a C-terminal hydrophobic region, which is thought to be inserted into membranes (Krappa et al., 1999). It has been demonstrated that evectin-2 is necessary for retrograde transport of Golgi proteins TGN46 (Maxfield & McGraw, 2004) and GP73 (Puri et al., 2002) from REs to the TGN (Uchida et al., 2011). Furthermore, we have shown

that the PH domain of evectin-2 can specifically bind phosphatidylserine (PS) but not phosphatidic acid (PA), phosphatidylethanolamine (PE), phosphatidylinositol (PI), sulfatide or any of the phosphatidylinositol phosphates (PIPs) when these lipids are present on liposomes (Uchida *et al.*, 2011). The observation that the PH domain of evectin-2 shows weak affinity for PA and PE, which share the phosphate and phosphorylethanolamine moieties of PS, respectively (Fig. 1), reveals the strict ligand specificity of the evectin-2 PH domain. The PS enrichment in REs has been shown by biochemical (Gagescu *et al.*, 2000) and cell-biological (Uchida *et al.*, 2011; Fairn *et al.*, 2011) approaches and the high specificity of the evectin-2 PH domain for PS is required for the RE localization of evectin-2 (Uchida *et al.*, 2011).

Recently, we determined the X-ray crystal structure of the human evectin-2 PH domain in complex with *O*-phospho-L-serine, the head group of PS, and elucidated the molecular basis of the binding mechanism (Uchida *et al.*, 2011). This complex structure effectively explained the low affinity for sulfatide, PI and PIPs, but not for PA or PE. In the crystal of the complex there are two PH-domain molecules in the asymmetric unit; one is *O*-phospho-L-serine-bound and the other is unbound. The *O*-phospho-L-serine binding site of the unbound molecule is occupied by the neighbouring unbound molecule, which is related to the intermolecular packing interaction by the symmetry operation $(1 - x, y + 1/2, 1 - z)$ (Fig. 2*a*). This crystal packing leads to blockage of the binding site of the unbound molecule by steric repulsion between amino-acid residues (Pro50, Arg108, Thr109 and Asn110 of the neighbouring unbound molecule). The carboxyl O atoms of Asn110 of the neighbouring unbound molecule form hydrogen bonds to Thr14 N and Ile15 N. The side chain of Ile15 also forms hydrophobic interactions with the side chain of Pro50 of the neighbouring unbound molecule (Fig. 2*a*). Because of this crystal packing, the unbound molecule is not a suitable model for an ideal apo-form structure, in which the ligand-binding site would be free from crystal packing. In order to elucidate the molecular mechanism of ligand binding, it is necessary to compare the structures of the complex and such an ideal apo form.

In this study, we used X-ray crystallography to obtain a new apo-form structure of the human evectin-2 PH domain in which the ligand-binding site is free from crystal packing (Fig. 2*b*). By comparing the new apo-form structure with the ligand-bound structure, we found obvious ligand-induced conformational changes that offer structural insight into the selectivity of the PH domain against PA and PE.

## 2. Materials and methods

The PH domain of human evectin-2 was purified as described previously (Uchida *et al.*, 2011). Apo-form crystals were obtained after 3 d incubation at 289 K using the sitting-drop vapour-diffusion method with a mixture of 0.5 µl protein (8.16 mg ml$^{-1}$) in buffer consisting of 20 m*M* Tris–HCl pH 7.5 and 0.5 µl mother liquor consisting of 20%(*w/v*) polyethylene glycol monomethyl ether 5000, 0.1 *M* bis-tris–HCl pH 6.5.

**Table 1**
Data-collection and refinement statistics.

Values in parentheses are for the highest resolution shell.

| | |
|---|---|
| Data collection | |
| Space group | $P2_12_12_1$ |
| Unit-cell parameters (Å) | $a = 34.2$, $b = 54.3$, $c = 111.6$ |
| Wavelength (Å) | 1.0000 |
| Resolution (Å) | 100–1.75 (1.78–1.75) |
| $R_{merge}$ (%) | 0.062 (0.346) |
| $\langle I/\sigma(I)\rangle$ | 48.0 (8.5) |
| Completeness (%) | 99.9 (100.0) |
| Multiplicity | 7.0 (7.2) |
| Refinement | |
| Resolution (Å) | 32.8–1.75 |
| No. of reflections | 20575 |
| $R_{work}/R_{free}$ | 0.220/0.259 |
| No. of atoms | |
| Protein | 1901 |
| Waters | 139 |
| Average $B$ factors (Å$^2$) | |
| Protein | 21.7 |
| Waters | 30.3 |
| R.m.s. deviations | |
| Bond lengths (Å) | 0.007 |
| Bond angles (°) | 1.073 |

Prior to data collection, crystals were soaked in cryogenic solution [24%(*w/v*) polyethylene glycol monoethyl ether 5000, 0.1 *M* bis-tris–HCl pH 6.5, 13%(*v/v*) ethylene glycol] for a few seconds. X-ray diffraction data were collected on beamline BL-5A at the Photon Factory, KEK (Tsukuba, Japan). Data processing and reduction were carried out using the *HKL* program suite (Otwinowski & Minor, 1997). The data were subsequently processed using the *CCP*4 program suite (Winn *et al.*, 2011). Initial phases were determined by the molecular-replacement method using *MOLREP* (Vagin & Teplyakov, 2010) with a search model obtained from the PH domain in complex with *O*-phospho-L-serine (PDB entry 3aj4; Uchida *et al.*, 2011). An initial round of rigid-body refinement was performed with *REFMAC* v.5.5 (Murshudov *et al.*, 2011) in order to position the molecule more accurately in the cell. Subsequently, cycles of *REFMAC* v.5.5 maximum-likelihood positional and *B*-factor refinement were alternated with manual remodelling using *Coot* (Emsley & Cowtan, 2004) until the *R* and $R_{free}$ factors converged. Water molecules were added based on visual inspection of the electron-density map using *Coot*. Two molecules were present in the asymmetric unit. Data-collection and refinement statistics are summarized
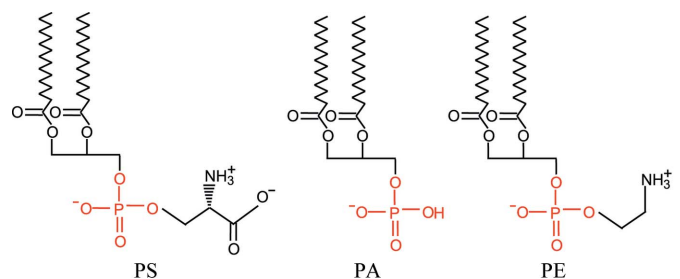


**Figure 1**
The chemical structures of PS, PA and PE are shown. Phosphate groups are indicated in red. For simplicity, only the dipalmitoyl (C16/C16) species are shown.

in Table 1. All figures were produced using *CCP4mg* (Potterton *et al.*, 2004). The intermolecular contact surface area was calculated using *AREAIMOL* implemented in the *CCP*4 program suite.

## 3. Results and discussion

### 3.1. New apo-form structure of the human evectin-2 PH domain

The apo-form structure obtained in this study contains two molecules (*A* and *B*) in the asymmetric unit. Superposition of the two molecules gives a root-mean-square (r.m.s.) deviation of 0.82 Å for 111 (99%) structurally equivalent C$^\alpha$ atoms. Thus, the two molecules exhibit overall similarity. The crystal-packing environments around the ligand-binding sites of molecules *A* and *B* are also similar. Contacts of neighbouring molecules are only observed at the outside of the ligand-binding site in the $\beta1$–$\beta2$ loop (Ser13–Arg18) of each molecule. The $\beta1$–$\beta2$ loop of molecule *A* makes contact with a neighbouring molecule *A* which is related by an intermolecular packing interaction with the symmetry operation ($x - 1$, $y + 1$, $z$); the intermolecular contact surface area is approximately 250 Å$^2$. The $\beta1$–$\beta2$ loop of molecule *B* makes contact with a neighbouring molecule *B* which is related by an intermolecular packing interaction with the symmetry operation ($x + 1$, $y + 1$, 0) (Fig. 2*b*); the contact surface area is approximately 202 Å$^2$. Details of these interactions are summarized in Table 2. In the following, we describe molecule *B* as the new apo-form structure because as described above the crystal-packing effects in molecule *B* are weaker than those in molecule *A*.

### 3.2. Comparison between apo-form and ligand-bound structures

We compared the new apo-form structure with previously determined apo and ligand-bound structures (Uchida *et al.*, 2011). The overall structures are similar to each other; however, the conformations of the ligand-binding sites located in the $\beta1$–$\beta2$ loop region are slightly different (Fig. 3). In the structure of the complex, Ser13 O$^\gamma$ forms hydrogen bonds to Lys17 N and Arg18 N, and Ser13 O is located near Lys17 N (at a distance of 3.2 Å), forming a possible hydrogen bond. Ser13 O$^\gamma$, Ile15 N and Leu16 N form a phosphate-binding pocket and form hydrogen bonds to phosphate

O3 of *O*-phospho-L-serine (Fig. 4*a*). This binding pocket does not exist in the unbound molecule of the complex. The carboxyl O atoms of Asn110 of the neighbouring unbound molecule make hydrogen bonds to Ser13 O$^\gamma$ and Ile15 N, and
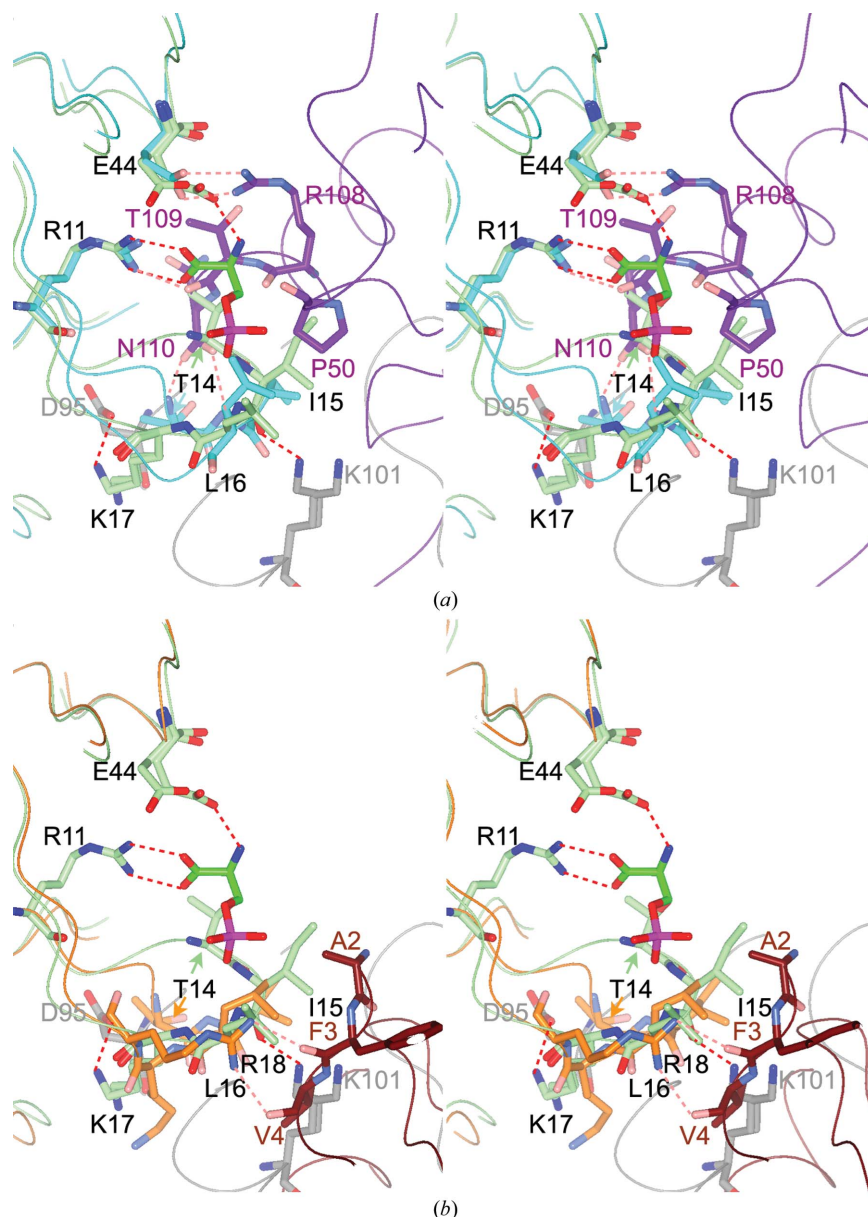


**Figure 2**
Crystal-packing effects on the $\beta1$–$\beta2$ loops of the human evectin-2 PH domain. *O*-Phospho-L-serine (stick model) is drawn with green C atoms, red O atoms and blue N atoms. (*a*) Stereoview of the superposition of the ligand-binding site of bound and unbound molecules of the *O*-phospho-L-serine complex (Uchida *et al.*, 2011; PDB entry 3aj4). The bound molecule is drawn with light green C atoms, red O atoms and blue N atoms. The neighbouring bound molecule is drawn with grey C atoms. Hydrogen bonds and salt bridges are shown as broken red lines. The unbound molecule is drawn with cyan C atoms, pink O atoms and light-blue N atoms. The neighbouring unbound molecule is drawn with purple C atoms. Hydrogen bonds and salt bridges in these structures are shown as broken pink lines. (*b*) Stereoview of the superposition of the ligand-binding site of the bound molecule of the *O*-phospho-L-serine complex (Uchida *et al.*, 2011; PDB entry 3aj4) and molecule *B* of the apo-form structure (this study). The bound molecule, neighbouring bound molecule, hydrogen bonds and salt bridges are drawn as described in (*a*). Molecule *B* is drawn with orange C atoms, pink O atoms and light blue N atoms. The neighbouring molecule *B* is drawn with brown C atoms. Hydrogen bonds and salt bridges in these structures are shown as broken pink lines.

**Table 2**
Interactions of the neighbouring molecule in the $\beta1$–$\beta2$ loop region.

The letters in parentheses represent the molecules.

| Residue | Residue in the neighbouring molecule | Distance (Å) | Interaction |
|---|---|---|---|
| Lys17 N$^\zeta$ (A) | Ser28 O (A) | 3.1 | Hydrogen bond |
| Arg18 N$^{\eta2}$ (A) | Val4 O (A) | 2.7 | Hydrogen bond |
| Ile15 C$^{\gamma2}$ (A) | Ala2 C$^\beta$ (A) | 3.7 | Hydrophobic interaction |
| | Ser28 C$^\beta$ (A) | 3.8 | Hydrophobic interaction |
| Ile15 C$^{\delta1}$ (A) | Ser0 C$^\alpha$ (A) | 4.1 | Hydrophobic interaction |
| Leu16 C$^{\delta2}$ (A) | Ala2 C$^\beta$ (A) | 3.7 | Hydrophobic interaction |
| Lys17 C$^\gamma$ (A) | Val4 C$^{\gamma2}$ (A) | 3.7 | Hydrophobic interaction |
| Arg18 N$^{\eta2}$ (B) | Phe3 O (B) | 2.8 | Hydrogen bond |
| Arg18 N$^{\eta1}$ (B) | Val4 O (B) | 2.9 | Hydrogen bond |
| Ile15 C$^{\gamma2}$ (B) | Ser28 C$^\beta$ (B) | 4.0 | Hydrophobic interaction |
| Leu16 C$^{\delta1}$ (B) | Ala2 C$^\beta$ (B) | 3.9 | Hydrophobic interaction |
| | Val4 C$^{\gamma2}$ (B) | 4.1 | Hydrophobic interaction |
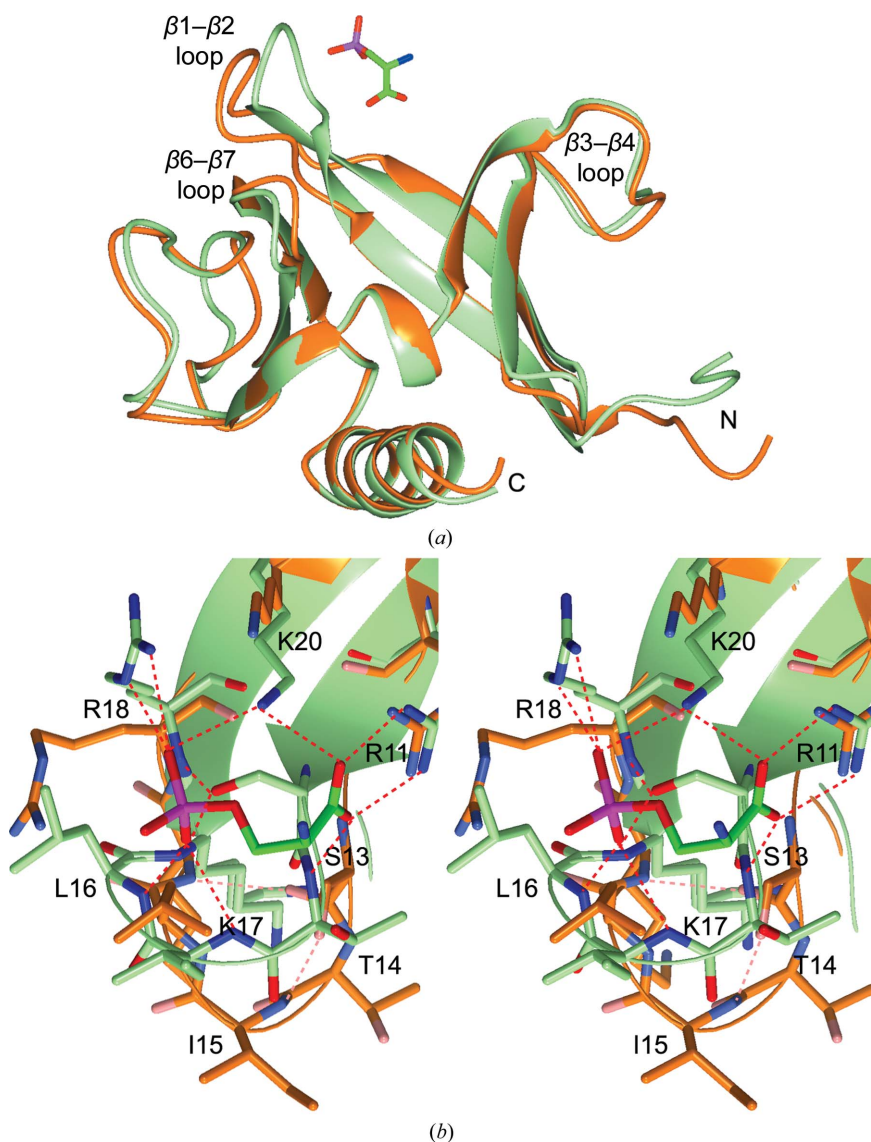


**Figure 3**
Superposition of the structures of the $O$-phospho-L-serine complex (light green) and the apo form (orange) of the human evectin-2 PH domain. $O$-Phospho-L-serine (stick model) is drawn with green C atoms and red O atoms. Representations are the same as in Fig. 2(b). (a) Overall structure represented as ribbon models. (b) Stereoview of the ligand-binding site.

part of the ligand-binding site is occupied (Fig. 4b). In contrast, in the ligand-binding sites of the new apo-form structure a hydrogen bond between Ser13 O$^\gamma$ and Ile15 N can be observed (Fig. 4c). This new apo-form structure reveals that a phosphate oxygen O3 binding pocket disappears and is replaced by a hydrogen bond between Ser13 O$^\gamma$ and Ile15 N.

### 3.3. The conformation of the $\beta1$–$\beta2$ loop differs between the structures of the new apo form and the complex

In addition to the striking conformational difference in the $\beta1$–$\beta2$ loop, we observed a change in the electrostatic surface potential at the ligand-binding site (Fig. 5). Residues Ser13–Arg18 undergo a conformational change, with movements of C$^\alpha$ atoms ranging from 0.9 Å at Arg18 to 5.5 Å at Thr14 (the movements for the other residues are 3.3 Å at Ser13, 4.6 Å at Ile15, 2.4 Å at Leu16 and 1.7 Å at Lys17). In the $O$-phospho-L-serine complex, the electron density of this loop is well ordered. The average $B$ factor of residues Ser13–Arg18 is 7.4 Å$^2$, which is almost the same as that of all residues (7.6 Å$^2$). In contrast, the electron density of this loop in the apo-form structure is poorly ordered and the average $B$ factor in the same region is 33.5 Å$^2$. This value is 1.4-fold higher than that of all residues in the apo form (24.0 Å$^2$). These observations suggest inherent flexibility of the $\beta1$–$\beta2$ loop in solution and also suggest that ligand binding promotes loop movement and stabilizes its conformation. This conformational change in the $\beta1$–$\beta2$ loop after ligand binding is generally similar to that observed in the PH domains of Bruton's tyrosine kinase (Baraldi et al., 1999) and Grp1 (Lietzke et al., 2000), the $\beta1$–$\beta2$ loops of which are stabilized by ligand binding.

The side chains of Arg18 and Lys20 interact with phosphate O2 and carboxyl O atom OT1 in the L-serine moiety of $O$-phospho-L-serine, respectively. The electron densities of these residues are more visible in the complex than in the apo form because of these interactions. Thus, ligand binding stabilizes this region. A similar observation was reported for residue Lys343 of the Grp1 PH domain, which recognizes P4 and P5 of the ligand (Lietzke et al., 2000).

### 3.4. Ligand-induced conformational change and strict ligand specificity of the human evectin-2 PH domain

The p47$^{phox}$ PX domain contains a second anion-binding pocket that may bind PA (Karathanassis et al., 2002). The wall of this pocket is formed by the side chains of His51, Lys55 and Arg70, giving it a basic character.

The NMR structure of the p47[phox] PX domain also shows that the surface is basic, mainly owing to the side chains of His51 and Lys55 (Hiroaki *et al.*, 2001). This observation implies that the pre-existence of a positively charged surface prior to ligand-induced conformational change may be necessary for high-affinity binding of PA. However, in our new apo-form structure of human evectin-2 PH domain no positively charged surface is present at the phosphate-binding site (Fig. 5a). This may explain why the human evectin-2 PH domain does not bind strongly to PA.

The positively charged side chain of Arg11, which recognizes the carboxyl group of *O*-phospho-L-serine in the structure of the complex, is exposed to the ligand-binding site in the

**Table 3**
Distances between the $C^\alpha$ atom of Ser13 and the $C^\alpha$ atoms of Ile15, Lys17 and Arg18.

| Residues | Apo-form structure (Å) | *O*-Phospho-L-serine complex (Å) |
|---|---|---|
| Ser13–Ile15 | 5.4 | 5.9 |
| Ser13–Lys17 | 5.4 | 4.4 |
| Ser13–Arg18 | 6.8 | 5.2 |

apo-form structure (Fig. 5a). In both structures the side chain of Arg11 is fixed by a hydrogen bond to $O^{\delta 2}$ of Asn22, which is conserved among evectin-2 PH domains from various species (Uchida *et al.*, 2011). These observations suggest that the side
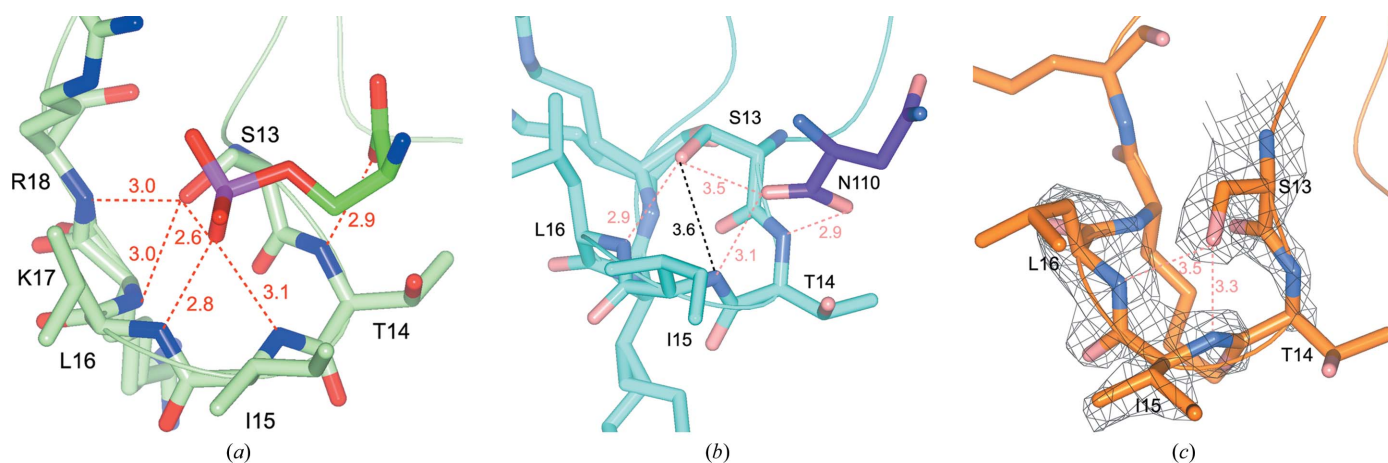


**Figure 4**
Ligand-binding sites of the human evectin-2 PH domain. Representations are as in Fig. 2. (*a*) Bound molecule of the *O*-phospho-L-serine complex. (*b*) Unbound molecule of the *O*-phospho-L-serine complex. The black broken line only indicates a distance, not a hydrogen bond. (*c*) New apo form (this study). A $\sigma_A$-weighted $F_o - F_c$ OMIT map (2.0$\sigma$ level; in grey mesh) is superposed on residues Ser13, Thr14, Ile15 and Leu16.
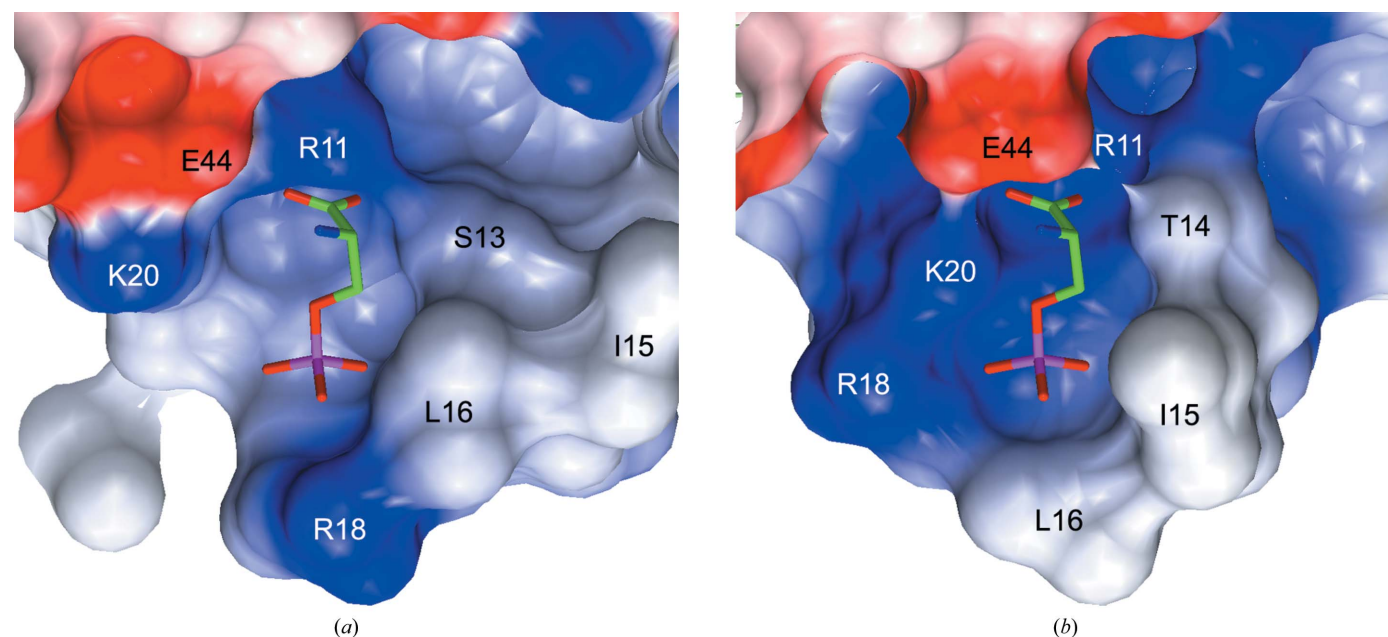


**Figure 5**
Charge-distribution surface models at the ligand-binding site. *O*-Phospho-L-serine is shown as a stick model (green C atoms, red O atoms and blue N atoms). The surface is coloured according to the electrostatic potential of the residues as calculated by *CCP4mg* (Potterton *et al.*, 2004; blue, +0.5 V; red, −0.5 V). (*a*) Charge-distribution surface model of the apo-form structure. *O*-Phospho-L-serine from the structure of the complex is superimposed. (*b*) Charge-distribution surface model of the *O*-phospho-L-serine complex.

chain of Arg11 first recognizes the carboxyl group of PS and anchors it to the surface of the protein. This might induce a conformational change of the $\beta1$–$\beta2$ loop *via* interactions between the main-chain N atom of Thr14 and the carboxyl group of PS. This mode of phospholipid interaction effectively explains why the evectin-2 PH domain does not strongly bind to PA and PE, as these lipids lack the carboxyl group of PS. In addition, conformational entropy may also be an important factor. Since the polar interaction cannot be formed in the case of PA and PE, the enthalpic contribution is less than in the case of PS. This low enthalpy may not be sufficient to overcome the conformational entropy associated with the change in the $\beta1$–$\beta2$ loop.

Furthermore, the ligand-induced conformational change of the $\beta1$–$\beta2$ loop is suitable for the formation of part of the phosphate-binding pocket. In the structure of the complex, Ser13 O$^\gamma$ forms hydrogen bonds to Lys17 N and Arg18 N; Ser13 O$^\gamma$, Ile15 N and Leu16 N form part of the phosphate-binding pocket and form hydrogen bonds to phosphate O3 of *O*-phospho-L-serine (Fig. 4*a*). Because Ser13 O$^\gamma$ forms hydrogen bonds to Ile15 N and Leu16 N in the apo-form structure (Fig. 4*c*), disruption of these hydrogen bonds is required in order to form the phosphate-binding region. These disruptions are achieved by the ligand-induced conformational change of the $\beta1$–$\beta2$ loop, as suggested by the distances between the C$^\alpha$ atoms of Ser13 and Ile15, Lys17 or Arg18 (Table 3).
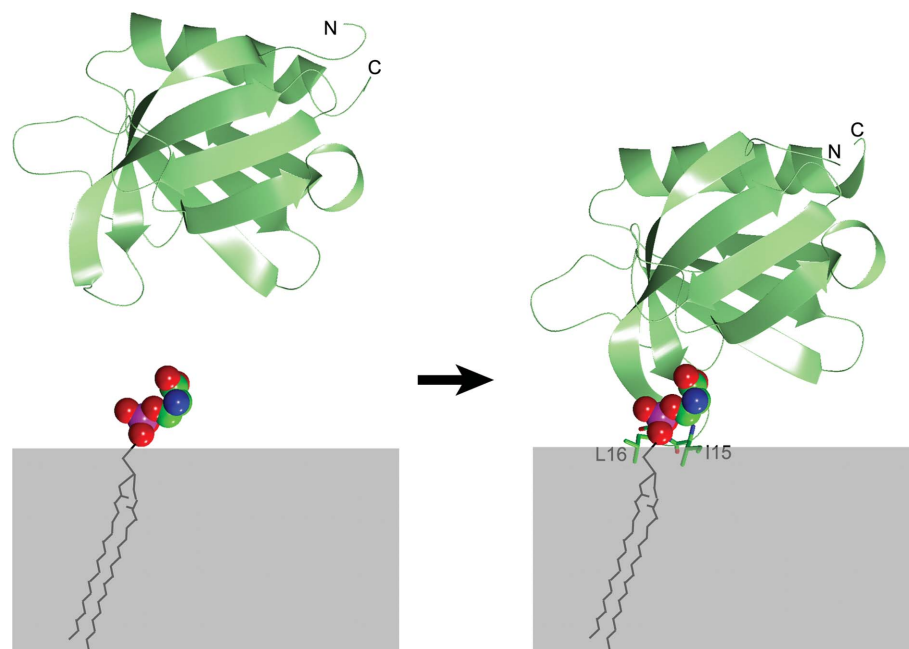


**Figure 6**
Model of lipid membrane binding mediated by PS. Human apo form (left panel) and ligand-bound (right panel) evectin-2 PH domains are drawn as light green ribbon diagrams. Side chains of the proposed membrane-interacting hydrophobic residues (Ile15 and Leu16) are drawn as stick diagrams. In PS, *O*-phospho-L-serine is depicted as a space-filling model. The lipid bilayer is depicted as a grey solid box.

### 3.5. Proposed membrane-binding model of human evectin-2 PH domain

Based on both the apo-form and complex structures and on reports of PS-binding domains (Stace & Ktistakis, 2006), we propose a model of membrane binding by the human evectin-2 PH domain mediated *via* PS (Fig. 6). Firstly, positively charged residues (Arg11, Arg18 and Lys20) are attracted by negatively charged carboxyl and phosphate groups of PS. Secondly, the O atoms of the carboxyl group of PS form salt bridges with the side chain of Arg11. Thirdly, ligand-induced conformational change occurs *via* the interaction between the carboxyl group of PS and Thr14 N. Ultimately, the hydrophobic side chains of Ile15 and Leu16 move to interact with the hydrophobic region of membrane lipids.

### 4. Conclusion

In this study, we determined a new apo-form structure of human evectin-2 PH domain in which the ligand-binding site is free from crystal packing. Based on this structure, we propose a plausible model for ligand-induced conformational change. The carboxyl moiety of the head group of PS is important for the ligand-induced conformational change, explaining the strict binding selectivity for PS and against PA and PE. Based on the structure, we have also proposed an overall model describing how human evectin-2 PH domain binds to specific lipid molecules on REs.

### References

Baraldi, E., Djinovic Carugo, K., Hyvönen, M., Surdo, P. L., Riley, A. M., Potter, B. V., O'Brien, R., Ladbury, J. E. & Saraste, M. (1999). *Structure*, **7**, 449–460.

Bonifacino, J. S. & Rojas, R. (2006). *Nature Rev. Mol. Cell Biol.* **7**, 568–579.

Emsley, P. & Cowtan, K. (2004). *Acta Cryst.* D**60**, 2126–2132.

Fairn, G. D., Schieber, N. L., Ariotti, N., Murphy, S., Kuerschner, L., Webb, R. I., Grinstein, S. & Parton, R. G. (2011). *J. Cell Biol.* **194**, 257–275.

Gagescu, R., Demaurex, N., Parton, R. G., Hunziker, W., Huber, L. A. & Gruenberg, J. (2000). *Mol. Biol. Cell*, **11**, 2775–2791.

Hiroaki, H., Ago, T., Ito, T., Sumimoto, H. & Kohda, D. (2001). *Nature Struct. Biol.* **8**, 526–530.

Johannes, L. & Popoff, V. (2008). *Cell*, **135**, 1175–1187.

Karathanassis, D., Stahelin, R. V., Bravo, J., Perisic, O., Pacold, C. M., Cho, W. & Williams, R. L. (2002). *EMBO J.* **21**, 5057–5068.

Krappa, R., Nguyen, A., Burrola, P., Deretic, D. & Lemke, G. (1999). *Proc. Natl Acad. Sci. USA*, **96**, 4633–4638.

Lietzke, S. E., Bose, S., Cronin, T., Klarlund, J., Chawla, A., Czech, M. P. & Lambright, D. G. (2000). *Mol. Cell*, **6**, 385–394.

Maxfield, F. R. & McGraw, T. E. (2004). *Nature Rev. Mol. Cell Biol.* **5**, 121–132.

Murshudov, G. N., Skubák, P., Lebedev, A. A., Pannu, N. S., Steiner, R. A., Nicholls, R. A., Winn, M. D., Long, F. & Vagin, A. A. (2011). *Acta Cryst.* D**67**, 355–367.

Otwinowski, Z. & Minor, W. (1997). *Methods Enzymol.* **276**, 307–326.

Potterton, L., McNicholas, S., Krissinel, E., Gruber, J., Cowtan, K., Emsley, P., Murshudov, G. N., Cohen, S., Perrakis, A. & Noble, M. (2004). *Acta Cryst.* D**60**, 2288–2294.

Puri, S., Bachert, C., Fimmel, C. J. & Linstedt, A. D. (2002). *Traffic*, **3**, 641–653.

Sandvig, K. & van Deurs, B. (2002). *Annu. Rev. Cell Dev. Biol.* **18**, 1–24.

Stace, C. L. & Ktistakis, N. T. (2006). *Biochim. Biophys. Acta*, **1761**, 913–926.

Uchida, Y. *et al.* (2011). *Proc. Natl Acad. Sci. USA*, **108**, 15846–15851.

Vagin, A. & Teplyakov, A. (2010). *Acta Cryst.* D**66**, 22–25.

Winn, M. D. *et al.* (2011). *Acta Cryst.* D**67**, 235–242.